Electronic Supplementary Information

Metal-organic framework derived carbon-confined Ni₂P nanocrystals supported on graphene for efficient oxygen evolution reaction

Manman Wang,[a] Mengting Lin,[a] Jiantao Li,[a] Lei Huang,[a] Zechao Zhuang,[a] Chao Lin,[a] Liang Zhou[*a] and Liqiang Mai[*a, b]

[a] *State Key Laboratory of Advanced Technology for Materials Synthesis and Processing, International School of Materials Science and Engineering, Wuhan University of Technology, Wuhan 430070, Hubei, China.*

[b] *Department of Chemistry, University of California, Berkeley, California 94720, United States.*

E-mail: mlq518@whut.edu.cn, liangzhou@whut.edu.cn

Experimental

Synthesis of Ni-MOF/rGO and Ni-MOF. Graphene oxide (GO) was prepared by a modified Hummers method.[1] Ni-MOF precursor was synthesized through a simple solvothermal method according to previous report.[2] Typically, 0.75 mmol of $Ni(NO_3)_2 \cdot 6H_2O$, 0.35 mmol of trimesic acid (BTC) and 750 mg of polyvinylpyrrolidone (PVP, K30) were dissolved in 36 mL of mixture solution (deionized water:methanol:DMF= 1:1:1, v/v/v) under continuous stirring. Then the obtained homogenous solution was transferred to a 50 mL Teflon-lined stainless steel autoclave and heated at 150 °C for 10 h. After washing and drying the precipitates, the Ni-MOF precursor was collected. The synthesis of Ni-MOF/rGO was almost the same with Ni-MOF except the change of mixture solution, the prepared mixture solution to synthesize Ni-MOF/rGO contained 10 mL of GO (2 mg mL^{-1}), 2 mL of deionized water, 12 mL of methanol and 12 mL of DMF.

Synthesis of Ni$_2$P@C/G and Ni$_2$P@C. The as-prepared Ni-MOF/rGO was annealed at 450 °C for 0.5 h in Ar with a heating rate of 1 °C min^{-1} to obtain the Ni@C/G. Then the obtained Ni@C/G was phosphorized by thermal decomposition of $NaH_2PO_2 \cdot H_2O$ under Ar atmosphere. 50 mg of Ni@C/G and 500 mg of $NaH_2PO_2 \cdot H_2O$ were put at two different quartz boats and heated to 300 °C for 2 h in Ar with a heating rate of 2 °C min^{-1}. After cooling to room temperature, the resulting products were washed with water and ethanol several times to remove the impurities and dried in vacuum at 60 °C. The preparation of Ni$_2$P@C was under the same process.

Synthesis of graphene. The graphene was synthesized via the same phosphorization process of Ni$_2$P@C/G, the dried GO powder was first annealed at 450 °C and followed by phosphorization process at 300 °C under Ar atmosphere.

Materials characterization. XRD patterns were recorded on a Bruker D8 Discover X-ray diffractometer with Cu Kα radiation (λ = 1.5418 Å). Field emission scanning electron microscopy (FESEM, JEOL JSM-7100F) and transmission electron microscopy (TEM, TECNAI G2 F30S-TWIN) were employed to characterize morphologies of the samples. The elemental mapping was collected by the TEM equipped with an energy-dispersive X-ray spectroscope

(EDS). X-ray photoelectron spectroscopy (XPS) measurements were performed on a Thermo Scientific, ESCALAB 250Xi system. CHNS/O elemental analyzer was applied to determine the carbon content. The Brunauer-Emmett-Teller (BET) specific surface area was obtained using a Tristar-3020 instrument.

Electrochemical measurements. Electrochemical measurements were conducted on a CHI 760D electrochemical workstation using a three-electrode system. Glassy carbon (GC) electrode with a diameter of 5 mm was used as the working electrode. The catalyst ink was prepared by dispersing 5 mg of catalyst into 1 mL of mixed solution consisting of 50 μL of 5 wt% Nafion, 800 μL of isopropanol and 150 μL of deionized water. Then the catalyst was loaded on the GC electrode by drop-casting 10 μL of ink to reach a loading of 0.25 mg cm^{-2}. A platinum wire electrode and saturated calomel electrode (SCE) were used as counter and reference electrodes, respectively. All the electrochemical data were recorded in 1 M KOH (PH= 13.62) electrolytes and potentials were converted to a reversible hydrogen electrode (RHE) via the equation: E(RHE) = E(SCE) + (0.24 + 0.0592 pH). Before evaluating the OER activity, catalysts were activated by 100 cyclic voltammetry (CV) cycles across the potential window of 1.2 − 1.8 V vs. RHE at a scan rate of 50 mV s^{-1}. Following the pre-activation process, linear sweep voltammetry (LSV) was performed at a scan rate of 5 mV s^{-1}. *iR* drop was corrected using the uncompensated series resistance collected from electrochemical impedance spectroscopy (EIS) at a potential of 0.55 V vs. SCE with frequency from 1 to 10^5 Hz. The long-term stability tests were measured by chronopotentiometry at the current density of 10 mA cm^{-2}. The electrochemically active surface area (ECSA) was determined by the double layer capacitance (C$_{dl}$). To obtain the C$_{dl}$ value, CV measurements were performed in non-Faradaic region at different scan rates (4, 8, 12, 16, 20, 40, 60, 80 and 100 mV s^{-1}). Then C$_{dl}$ was estimated by plotting the ΔJ = (J$_a$ - J$_c$) against the scan rate. The linear slope is equivalent to twice of the C$_{dl}$.The turnover frequency (TOF) values were calculated from the equation:

$$TOF = \frac{jA}{4Fn}$$

where *j* is the current density at an overpotential of 350 mV, A is the surface area of the

glassy carbon electrode, the number 4 means four electrons per mol of O_2, F is the Faraday constant and n is the number of moles of the active sites on the electrode. In our work, we regard Ni atoms as the active sites, and do not consider the non-metallic atoms as active sites, so the graphene and carbon are ignored when calculating the TOF value of $Ni_2P@C/G$ and $Ni_2P@C$. What's more, the graphene shows the highest overpotential (360 mV) to reach 10 mA cm^{-2} and almost does not catalyze the oxidation of water at the overpotential of 350 mV. Compared to $Ni_2P@C$, and the TOF value of graphene (0.00079 s^{-1}, based on the carbon atoms) is negligible.
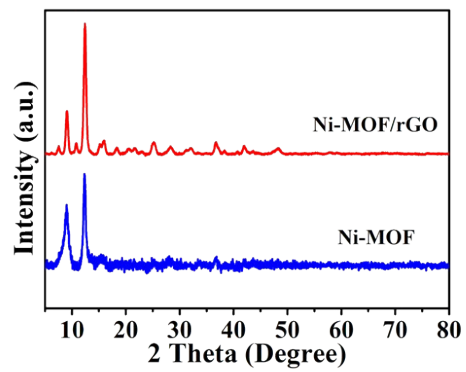
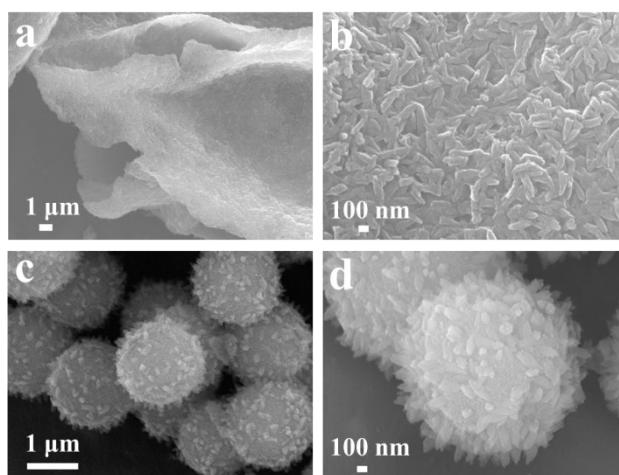**Fig. S1** XRD patterns of Ni-MOF/rGO and Ni-MOF.

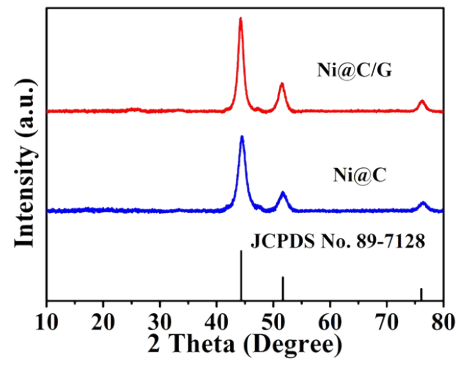**Fig. S2** SEM images of (a, b) Ni-MOF/rGO and (c, d) Ni-MOF.
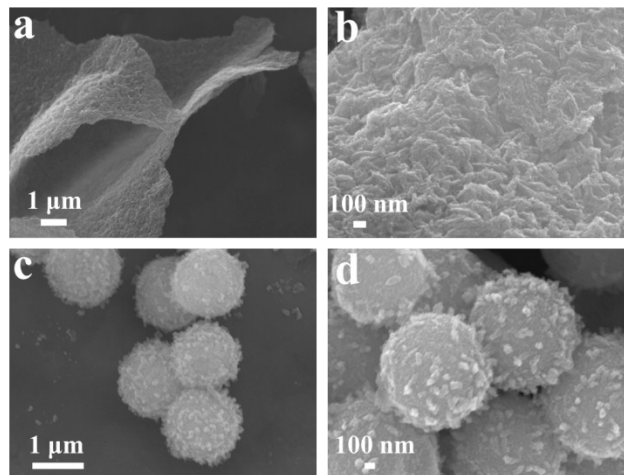
Fig. S3 XRD patterns of Ni@C/G and Ni@C.

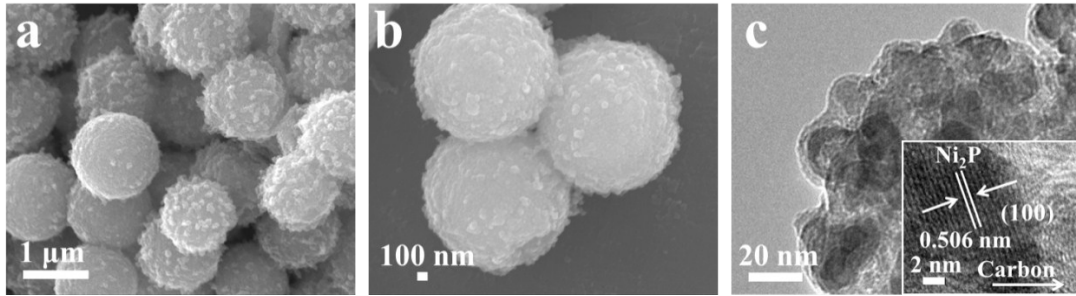**Fig. S4** SEM images of (a, b) Ni@C/G and (c, d) Ni@C.

Fig. S5 (a, b) SEM images of $Ni_2P@C$. (c) TEM image of $Ni_2P@C$. The inset is the HRTEM image of $Ni_2P@C$.
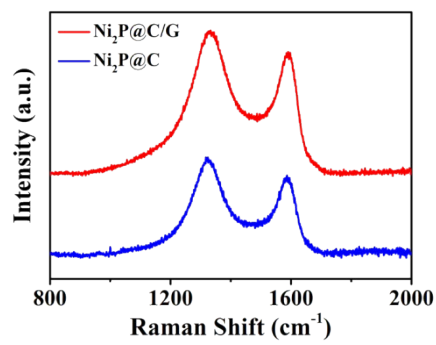
Fig. S6 Raman spectra of $Ni_2P@C/G$ and $Ni_2P@C$.
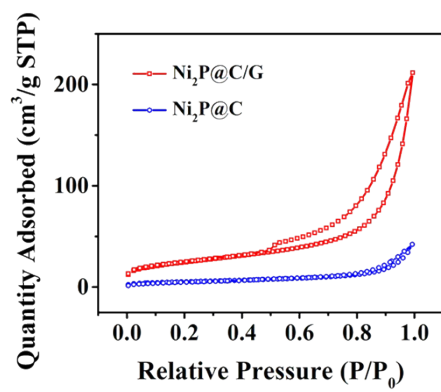
Fig. S7 N_2 adsorption-desorption isotherm of the $Ni_2P@C/G$ and $Ni_2P@C$.
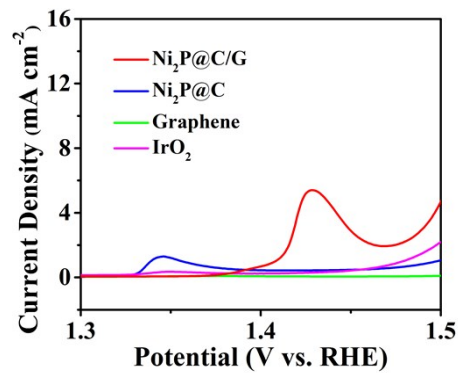
Fig. S8 Enlargement of the anodic peaks in LSV curves**.**

Owing to the less exposed active sites, $Ni_2P@C$ possesses much smaller anodic peak area than the $Ni_2P@C/G$, so the anodic peak for $Ni_2P@C$ is not that obvious when compared with $Ni_2P@C/G$.
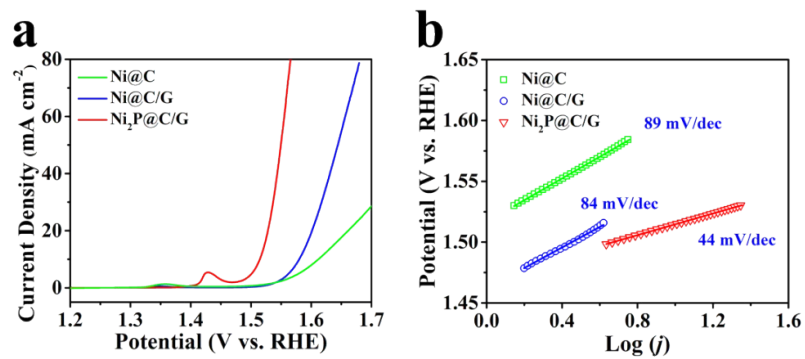

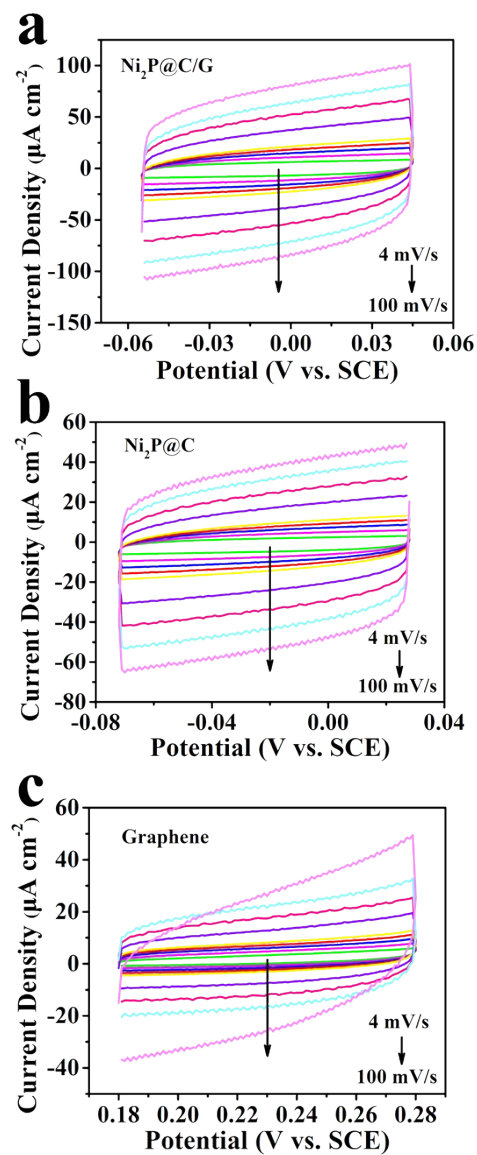**Fig. S9** (a) LSV curves and (b) Tafel plots of Ni@C, Ni@C/G and $Ni_2P@C/G$.

Fig. S10 Cyclic voltammograms (CVs) of (a) $Ni_2P@C/G$, (b) $Ni_2P@C$ and (c) graphene at different scan rates from 4 to 100 mV s^{-1}.
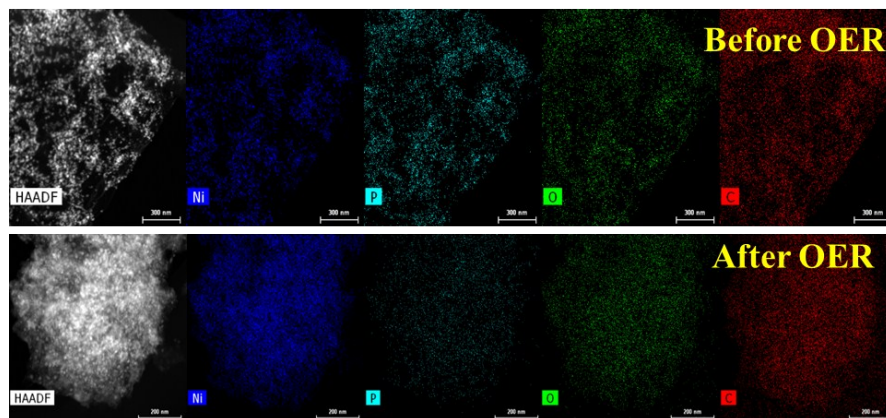
Fig. S11 HAADF-STEM images and corresponding elemental mapping before and after OER stability test in 1 M KOH for 10 h.
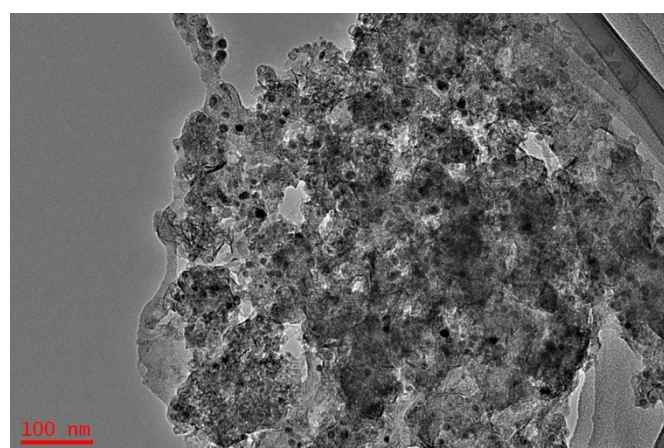

Fig. S12 TEM image of Ni$_2$P@C/G after OER stability test in 1 M KOH for 10 h.

Table S1. Comparison of the electrocatalytic activity for several recently reported non-noble OER catalysts in alkaline solution.

Catalysts	Electrolyte	Loading (mg cm^{-2})	η@10 mA cm^{-2} (mV)	Tafel slope (mV dec^{-1})	TOF(s^{-1})	References
Ni$_2$P@C/G	1 M KOH	0.25	285	44	0.1 η = 350 mV	**This work**
Ni$_2$P@C	1 M KOH	0.25	340	68	0.01 η = 350 mV	**This work**
Ni-P	1 M KOH	0.20	300	64	—	[3]
Ni$_2$P nanoparticles	1 M KOH	0.14	290	59	—	[4]
Ni$_2$P nanowires	1 M KOH	0.14	330	47	—	[4]
α-Ni(OH)$_2$ hollow spheres	0.1 M KOH	0.20	331	42	0.0361 η = 350 mV	[5]
N-doped 3D crumpled graphene-CoO	1 M KOH	0.70	340	71	—	[6]
CoMnP nanoparticles	1 M KOH	0.284	330	61	—	[7]
CoSe$_2$ nanosheets	0.1 M KOH	0.142	320	44	0.33 η = 500 mV	[8]
CeO$_2$/CoSe$_2$ nanobelt	0.1 M KOH	0.20	288	44	—	[9]
Ni$_3$N nanosheets	1 M KOH	0.285	—	45	—	[10]
NiCo$_2$O$_4$ nanosheets rich in oxygen vacancies	1 M KOH	0.285	320	30	0.072 η = 360 mV	[11]
FeNC sheets/NiO	0.1 M KOH	0.24	390	76	0.2 η = 350 mV	[12]

All the above catalysts were loaded on glassy carbon.

References

1. H. Wang, Y. Yang, Y. Liang, J. T. Robinson, Y. Li, A. Jackson, Y. Cui and H. Dai, *Nano Lett.*, 2011, **11**, 2644-2647.
2. F. Zou, Y. M. Chen, K. Liu, Z. Yu, W. Liang, S. M. Bhaway, M. Gao and Y. Zhu, *ACS Nano*, 2016, **10**, 377-386.
3. X. Y. Yu, Y. Feng, B. Guan, X. W. D. Lou and U. Paik, *Energy Environ. Sci.*, 2016, **9**, 1246-1250.
4. L. A. Stern, L. Feng, F. Song and X. Hu, *Energy Environ. Sci.*, 2015, **8**, 2347-2351.
5. M. Gao, W. Sheng, Z. Zhuang, Q. Fang, S. Gu, J. Jiang and Y. Yan, *J. Am. Chem. Soc.*, 2014, **136**, 7077-7084.
6. S. Mao, Z. H. Wen, T. Z. Huang, Y. Hou and J. H. Chen, *Energy Environ. Sci.*, 2014, **7**, 609-616.
7. D. Li, H. Baydoun, C. N. Verani and S. L. Brock, *J. Am. Chem. Soc.*, 2016, **138**, 4006-4009.
8. Y. W. Liu, H. Cheng, M. J. Lyu, S. J. Fan, Q. H. Liu, W. S. Zhang, Y. D. Zhi, C. M. Wang, C. Xiao, S. Q. Wei, B. J. Ye and Y. Xie, *J. Am. Chem. Soc.*, 2014, **136**, 15670-15675.
9. Y. R. Zheng, M. R. Gao, Q. Gao, H. H. Li, J. Xu, Z. Y. Wu and S. H. Yu, *Small*, 2015, **11**, 182-188.
10. K. Xu, P. Z. Chen, X. L. Li, Y. Tong, H. Ding, X. J. Wu, W. S. Chu, Z. M. Peng, C. Z. Wu and Y. Xie, *J. Am. Chem. Soc.*, 2015, **137**, 4119-4125.
11. J. Bao, X. D. Zhang, B. Fan, J. J. Zhang, M. Zhou, W. L. Yang, X. Hu, H. Wang, B. C. Pan and Y. Xie, *Angew. Chem., Int. Ed.*, 2015, **54**, 7399-7404.
12. J. Wang, K. Li, H. X. Zhong, D. Xu, Z. L. Wang, Z. Jiang, Z. J. Wu and X. B. Zhang, *Angew. Chem., Int. Ed.*, 2015, **54**, 10530-10534.